Journal of
Materials Chemistry C

Materials for optical, magnetic and electronic devices

Accepted Manuscript

This article can be cited before page numbers have been issued, to do this please use: C. B. Auti, A. G. Chakkar, S. Semwal, S. Selter, Y. Shemerliuk , B. Büchner, S. Aswartham, K. Pal and P. Kumar, *J. Mater. Chem. C*, 2026, DOI: 10.1039/D5TC03093E.

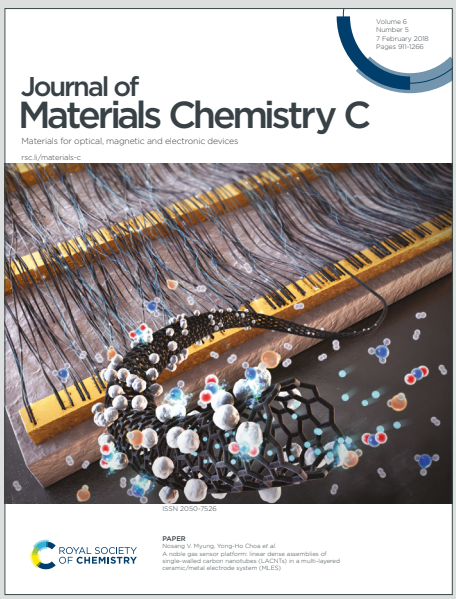

ROYAL SOCIETY OF CHEMISTRY

rsc.li/materials-c

DOI: 10.1039/D5TC03093E

Antipolar and short and long-range magnetic ordering in quasi-two-dimensional $AgCrP_2S_6$

Chaitanya B. Auti[1,*], Atul G. Chakkar[1], Shantanu Semwal [2], Sebastian Selter[3], Yuliia Shemerliuk[3], Bernd Büchner[3,4], Saicharan Aswartham[3], Koushik Pal[2], and Pradeep Kumar[1#]

[1]*School of Physical Sciences, Indian Institute of Technology, Mandi-175005, India.*

[2]*Department of Physics, Indian Institute of Technology Kanpur, Kanpur 208016, India*

[3]*Institute for Solid State Research, Leibniz IFW Dresden, Helmholtzstr. 20, 01069 Dresden, Germany*

[4]*Institute of Solid State and Materials Physics and Würzburg-Dresden Cluster of Excellence ct.qmat, Technische Universität Dresden, 01062 Dresden, Germany*

Abstract

$AgCrP_2S_6$ provides a versatile playground to probe dynamics of the quasiparticle excitations as well as multiple phase transitions with lowering temperature linked with the polar, lattice and spin degrees of freedom. Here, we report an in-depth temperature- and polarization-dependent Raman scattering measurements on single crystals of quasi 2D zigzag antiferromagnet $AgCrP_2S_6$ along with the first principle based phonon calculations. We observed multiple phase transitions triggered by the short and long-range ordering of spins at ~ 90 K and 20 K, respectively; within the Cr sublattice where spins are arranged in a 1D chain, evident by the distinct anomalies in the phonon modes self-energy parameters as well as intensity. Contrary to the conventional belief, we proposed the possibility of quasi-antipolar ordering at ~ 200 K and with further lowering in temperature an antipolar ordering at ~ 140 K attributed to the Ag ions, which is conjectured to be forbidden owing to the heaviness of Ag ions. The quasi-antipolar and antipolar ordering is gauged via the distinct renormalization of the phonon's parameters, which survives at all the temperatures. Additionally, large number of modes appears with decreasing the temperature, in the window of ~ 200-140 K, where antipolar ordering starts settling in. The emergence of large number of phonon modes below ~ 200 K, nearly double of those at room temperature, suggests the lowering of symmetry from high temperature C_{2h} to the low temperature C_2 or C_s.

*autichaitanya5@gmail.com

#pkumar@iitmandi.ac.in

View Article Online
DOI: 10.1039/D5TC03093E

1. Introduction

Two-dimensional (2D) van der Waals (vdWs) materials have attracted significant attention due to their distinct properties that are advantageous for potential applications in next-generation electronics as well as rich physics [1,2]. A significant domain of modern research focuses on magnetic vdWs materials that display intriguing physical properties. The intrinsic 2D nature of these materials opens up unique opportunities to explore novel magnetic ground states, magnetic excitations, and their interactions with other quasiparticle excitations [3-6]. These tunable properties are of great interest not only for fundamental studies but also for potential applications in advanced fields such as spintronics, optoelectronics, and nanoelectronics [7,8].

Recently, 2D metal thiophosphates (MTPs) have drawn significant interest because of their intriguing characteristics, including magnetism down to monolayer, ferroelectricity, and multiferroicity. The MPS_3 (M = Mn, Fe, Ni, Co, V) family of layered materials presents a rich array of isostructural compounds that form 2D vdWs antiferromagnets [6,9,10]. 2D MPS_3 materials exhibit a wide range of band gaps (~ 0.24-3.5 eV), which makes them highly promising for applications in catalysis, spintronic, and energy conversion devices [11]. Colombet et al. reported that heterocharge substitution also yields numerous stable compounds, which provide an extra degree of freedom in the atomic arrangement [12,13]. One such member of this family is $AgCrP_2S_6$, which exhibits an antiferromagnetic transition temperature (T_N) at ~ 20 K [14]. The non-magnetic Ag atom and the magnetic Cr atom are arranged in zigzag strips. The Ag^+ ion has bigger size compared to the Cr^{3+} ion; as a result, the layer above the Ag

View Article Online
DOI: 10.1039/D5TC03093E

atoms significantly bends outward (see Supplemental Material Fig. S1-(a) [15]). Consequently, a deformation occurs in the P_2S_6 octahedra to accommodate the different sizes of the cations. Therefore, to reduce this strain energy, the cations organize themselves in a zigzag chain formation, this arrangement functions as a one-dimensional chain of magnetic atoms with a spin value of S = 3/2 (see Supplemental Material Fig. S1-(d) [15]). The layers are arranged in AAA stacking, resulting in a quasi-2D structure [16,17].

Magnetic fluctuations in 2Ds are influenced by the symmetry of the order parameters, namely the Ising, XY, and Heisenberg types [9]. One-dimensional (1D) spin S = 3/2 Heisenberg antiferromagnetic Hamiltonian is given as [18] :

$H = -J\sum_i (S_i^x S_{i+1}^x + S_i^y S_{i+1}^y + \lambda S_i^z S_{i+1}^z) + J'\sum_{i,k} S_i S_k + D\sum_i (S_i^z)$, where λ and D denotes the exchange and single-ion anisotropy parameters, S_i^x, S_i^y and S_i^z are the x, y, and z components of the total spin at $_i$ th site. *J* and *J′* are the intra- and interchain exchange coupling constants, respectively. A very small value of $|J'/J| \sim 10^{-4}$ (for $AgCrP_2S_6$) confirm that the system comprises of 1D spin chains. The Cr-(P or S)-Cr angle of around 90^0 allows a strong direct overlap of the octahedrally surrounded Cr's half-filled t_{2g} orbitals [18]. Recent work by Park et al. [19] also suggests that the weakest interaction is interchain, leading to essentially 1D magnetic behaviour in each layer, while two layers exhibit a weak ferromagnetic coupling. The anisotropic structure introduces an additional degree of freedom, offering the potential to manipulate the material's structure in different ways to provide tunability for probing fundamental magnetism with reduced dimensionality.

Raman spectroscopy is a powerful technique for studying the presence of magnons, phase transitions, and various quasiparticle excitations, including spin-phonon and electron-phonon coupling, in 2D magnetic materials [20-24]. Recently, heterocharge MTPs moved into focus due to their low-dimensional magnetism, multiferroicity, and Haldane phase [25,26].

View Article Online
DOI: 10.1039/D5TC03093E

Understanding these singular behaviour in MTPs will provide valuable insights for potential applications in spin-based logic gate devices, non-volatile memory storage devices, and the possibility of fabricating heterostructures for multifunctional device applications [27,28]. Motivated by the rich underlying physics in these low-dimensional systems, we conducted an in-depth investigation of the $AgCrP_2S_6$ single crystal using Raman scattering measurements as well as first principle calculations of the phonons. The absence of current literature on the temperature-dependent characteristics of the phonon and magnetic dynamics, suggesting a potential for uncovering novel insights into materials vibrational as well as magnetic properties.

In this work, we elucidate the phonon excitations and crystal symmetry of $AgCrP_2S_6$ using comprehensive temperature and polarization-dependent Raman spectroscopy measurements along with the first principle calculations of the phonons. We observed significant hardening of the low energy phonon modes, attributed to the strong phonon-phonon anharmonic interactions, or an increase in bonding stiffness, indicating structural instability in the material. Based on the temperature-dependent phonon modes analysis, we observed a signature of antiferromagnetic transition at T_N~ 20 K. Interestingly, we observed anomalies in mode frequency, linewidth, and intensity around temperatures ~ 90 K, ~ 140 K, and ~ 200 K. These transitions are attributed to the possible short-range ordering of the spins and polar ordering in the system, respectively. We also examined the interactions between quasiparticle excitations and electronic and/or magnetic continuums, i.e., Fano asymmetry in the phonon line shape, as a function of temperature. Polarization-dependent measurements show the two-fold symmetry of all observed modes in line with the group theoretical predictions. Quite surprisingly we also observed a systematic rotation of the polarization major axis of the phonon modes as a function of temperature. This opens possibility of the tunability of the scattered light in this quasi 2D magnet via symmetry control.

2. Experimental and computational details

View Article Online
DOI: 10.1039/D5TC03093E

2.1. Experimental details

The single crystal samples of $AgCrP_2S_6$ were prepared by using chemical vapor transport technique as described in reference [29]. Temperature-dependent Raman scattering and photoluminescence (PL) measurements (see Supplemental Material for PL measurements [15]) were carried out from 6 to 300 K with ±0.1 K precision with Closed-Cycle Refrigerator (Montana) and the Horiba LabRAM HR-Evolution Raman spectrometer in the backscattering configuration. A 633 nm laser was used to excite the Raman spectra. Laser power was kept very low (< 0.5 mW) to prevent local heating. A 50X (NA=0.5) long working distance objective was used to focus the incident laser light on the sample. Scattered light was collected through a Peltier-cooled charge-coupled detector. To unveil the symmetry of phonon modes, polarization-dependent measurements were performed at temperatures of 6 K, 60 K, 120 K, and 170 K. A half-wave plate was placed near the laser entrance to manually rotate the incident polarization onto the sample, while the scattered polarization analyzer remained fixed.

2.2. Computational details

We performed first-principles density functional theory (DFT) calculations using the Vienna Ab initio Simulation Package [30,31] and utilized pseudo potentials generated using the projected augmented wave (PAW) [32] method. The valence electron configurations used are $4p^6 4d^{10} 5s^1$, $3d^5 4s^1$, $3s^2 3p^3$, $3s^2 3p^4$ for Ag, Cr, P and S respectively. We used gaussian smearing for treating the partial occupancies for each orbital with energy broadening of 0.05 eV and treated the exchange-correlation energies of the electrons within the GGA Perdew-Burke-Ernzerhof (PBE) functional [33]. The cutoff for the kinetic energy was set to 450 eV for all calculations. The primitive cell structure of $AgCrP_2S_6$ contained 20 atoms (2 Ag, 2 Cr, 4 P and 12 S atoms), we considered the antiferromagnetic (AFM) arrangement of Cr atoms and used the DFT-D3 method of Grimme [34] to include the vdW interactions in the structure. The lattice parameters were fully optimized using a k-point grid of 9x9x9 and the energy

View Article Online
DOI: 10.1039/D5TC03093E

convergence criteria was set to 10^{-8} eV. After full optimization the energies are converged and the force on each atom is of the order of 10^{-4} eV/A or less. The lattice parameters and volume for the optimized structure were a=5.888 A, b=10.647 A, c=6.704 A and 403.848 A^3, respectively. The changes of a, b, c and volume are 0.09%, 0.24%, -0.6% and 0.3%, respectively when compared with the experimental lattice parameters.

The phonon calculations were done using the finite-difference method as implemented in Phonopy [35,36]. We used a 2x2x2 supercell containing 160 atoms, considering AFM arrangement of Cr atoms and including the vdW interactions. The tabulated frequencies and symmetry labels of all the modes at Γ - point are provided in Table S2.

3. Results and discussion

3.1 Crystal structure and phonon modes

$AgCrP_2S_6$ exhibits monoclinic symmetry having space group *P2/a* (#13) and point group C_{2h} (2/m). Unit cell of the $AgCrP_2S_6$ bulk single crystal consists of 60 phonon modes at the Γ - point of the Brillouin zone, with the following irreducible representations [37]: $\Gamma_{total} = 14A_g + 14A_u + 16B_g + 16B_u$. There are 30 Raman active ($\Gamma_{Raman} = 14A_g + 16B_g$) modes and 27 infrared active ($\Gamma_{IR} = 13A_u + 14B_u$) modes (for more details see Table I). The Raman spectra is recorded using 633 nm laser excitation, and 48/27 Raman modes are observed at 6 K/300 K, which are labelled as P1-P48 at 6 K, as shown in Fig. S2. To extract the self-energy parameters of phonon modes, i.e., peak frequency (ω), full width at half maximum (FWHM), and intensity, spectra are fitted using a sum of Lorentzian functions. We also recorded spectra in the higher frequency range of 700-1400 cm^{-1} and observed some very weak higher order modes, as shown in Supplemental Material Fig. S9 [15]. Figure 1(a) and 1(b) shows the temperature evolution of the Raman spectrum of $AgCrP_2S_6$ in the temperature range 6 to 300

View Article Online
DOI: 10.1039/D5TC03093E

K from 15-350 cm^{-1} and 350-700 cm^{-1} (magnified spectra in the smaller spectral range is shown in Supplemental Material Fig. S6, Fig. S7, and Fig. S8 [15]).

All higher frequency modes ranging from ~ 250 cm^{-1} are softens with increasing temperature, showing normal anharmonic phonon behaviour; while some lower frequency range modes show anomalous hardening, and others show a softening and get broadened with increasing the temperature. In the $M_2P_2S_6$ material family, the higher frequency (above ~ 250 cm^{-1}) modes are assigned to the vibration due to (P_2S_6) octahedra; therefore, these modes are similar in all $M_2P_2S_6$ compounds, and the lower frequency (below ~ 250 cm^{-1}) Raman modes are assigned to the heavy metal ion [38]. The particular M atom determines the cutoff frequency that separates the high- and low-frequency regimes. Phonon dispersion along with the atom resolved phonon density of state (phdos) is shown in Fig. 2a and Fig. 2b, respectively. From the atom resolved phdos in Fig. 2b we can see that in the high frequency region (500 cm^{-1} to 650 cm^{-1}), the contributions to the phonon dispersion are mainly due to the P and S atoms due to smaller masses of these atoms. In the middle region (150 cm^{-1} to 500 cm^{-1}) region we see the P contribution waning and being taken over by the S atoms and rising contribution due to Cr seen around 350 cm^{-1}, 300 cm^{-1}, and at 200 cm^{-1}. Finally at the lower frequency region (20 cm^{-1} to 150 cm^{-1}) we see the contribution of S, P and Cr decreasing and increasing Ag contributions with large Ag localization with peaks around 60 cm^{-1} and 20 cm^{-1} to 40 cm^{-1}. All prominent phonon modes intensity reduces drastically from the lowest recorded temperature to the highest temperature as shown in Fig. 1(a) and 1(b). The most intense phonon mode P19 could be a mode associated with the anionic complex $[P_2S_6]^{4-}$, which is almost twice as intense as the other prominent modes P11, P33, and P47. Many phonon modes as P4, P5, P9, P15, P16, P17, P20, P23, P25, P29, P20, P31, P32, P34, P35, P36, P40, P41, P42, P44, and P48 disappear with increasing the temperature, see Fig. S3, which shows disappeared phonon

modes. Mode P31 (~ 469.5 cm^{-1} at 6 K) shows an asymmetric line shape (see Fig. 4(c)), discussed in detail in Sec. 3.4.

3.2 Temperature dependence of the phonon modes

Generally, mode frequencies are expected to exhibit softening with increasing temperature [39]. Figure 3 shows the temperature dependence of frequency and FWHM of some of the prominent phonon modes labelled as P2, P3, P5, P7, P8, and P10-P14. (For more phonon modes, see Supplemental Material Fig. S4 [15]). Some intriguing features are observed: (i) For the lower frequency range $\omega \leq 250$ cm^{-1}, some of the phonon modes P2, P3, P7, P10, P12, and P14 show abnormal hardening with increasing the temperature. (ii) Rapid decrease of intensity of the phonon modes P10 and P14 with increasing the temperature (see Fig. 4(a)). (iii) Many phonon modes disappear with increasing the temperature (see Supplemental Material Fig. S3 [15]). Interestingly, mode P7 shows abnormal hardening with increasing the temperature and approaches towards P8 (ω_{P8} = 159.5 cm^{-1} at room temperature). Mode P10 approaches towards P11 with a sharp increase of frequency $\Delta\omega_{P10}$ ~ 12 cm^{-1}. However, P13 and P14 diverge from each other with increasing temperature (see Fig. 4(b)). P2 and P3 both show abnormal hardening with increasing the temperature. These modes may be associated with heavy metal ion Ag^{+} [16]. The possible reasons associated with the anomalous frequency change are discussed in detail in Sec. 3.3.

3.2.1 Anomalous temperature dependence of the phonon modes

Interestingly, phonon mode P5, P6, P8, P12, P13, P14, P19, P21, and P47 exhibit anomalous softening in frequency below ~ 20 K, i.e., antiferromagnetic ordering T_N(~ 20 K). The FWHM of the modes P2, P3, P7, P8, P10, P13 also shows change in slope at ~ T_N. This anomalous nature of the phonon modes below T_N may be attributed to the spin-phonon

View Article Online
DOI: 10.1039/D5TC03093E

coupling. It is noted that spin-phonon coupling is generally expected to be effective only up to long range ordering temperature where the long-range magnetic correlations exist [40-42].

We note that at room temperature several phonon modes are relatively broad (see Fig. 1(a), 1(b), and Fig. S6-S8), evolving into much sharper modes at low temperature. While such behaviour is consistent with anharmonic phonon-phonon interactions, the relatively large linewidth changes observed for low frequency modes such as P2, P3, P7, P11, and P12 about ~ 75% ($\left|(\omega_{6K}-\omega_{300K})\right|/\omega_{300K}$),(see Fig. 3) may also suggest a possible contribution from additional temperature-dependent lattice fluctuations and the presence of Ag^{+} cation disorder at high temperature

It is noteworthy that several phonon modes P5, P6, P8, P13, P19, P21, P24, P28, P33, P39, and P47 show a change in the slope of their frequency shifts around ~ 90 K (see Fig. 3 and Fig. S4). Mode P3 exhibits a sharp frequency increase up to ~ 90 K, remaining nearly constant thereafter. The FWHM of modes P13, P28, P45, and P47 also changes slope near ~ 90 K, indicating a clear anomaly. In addition, mode P10 shows a slight kink near ~ 140 K, while modes P13, P19, and P21 display discontinuities in frequency at this temperature. The FWHM of phonon modes P6, P10, and P14 exhibits a jump near ~ 140 K, while modes P8, P19, and P47 show a change in slope, indicating an anomaly at this temperature. Around ~ 200 K, mode P2 displays a discontinuity in frequency, and modes P8, P19, P21, and P39 show slope changes in their frequency shifts. Mode P12 exhibits an unusual hardening behaviour above 200 K, with its frequency increasing from ~ 204.5 to ~ 209 cm^{-1} with increasing temperature from 200 K till ~ 300 K, marking a clear anomaly near 200 K. Additionally, the FWHM of modes P6 and P10 shows a jump, and that of modes P7, P12, P19, and P21 changes slope around this temperature, lifetime of the phonons is strongly influenced in the vicinity of this temperature. Also, many phonon modes start appearing below ~ 200 K and continue to emerge

View Article Online
DOI: 10.1039/D5TC03093E

till ~ 140 K (see Supplemental Material Fig. S3 [15]) consistent with the anomalies observed in the modes which survive at all the temperatures.

Interestingly, intensity change of all phonon modes with temperature is nearly uniform except for the modes P10 and P14 whose intensity decreases sharply with increasing temperature by ~ 10 times compared to its intensity at 6 K, as shown in Fig. 4(a). Phonon modes P2 and P3 show very interesting intensity variation; their intensity increases with increasing temperature up to ~ 90 K, after which it decreases, indicating an anomaly at ~ 90 K. We note that similar intensity behaviour is also reported for the low-frequency modes in a sister compound i.e. $CuCrP_2S_6$, which suggest that lattice dynamics of off-centre Cu^+ cations within the intralayer are not quenched, indicating order-disorder-type of structural transition is responsible for the emergence of defect dipoles associated with Cu ions [43]. It is observed that the intensity of the modes P7, P10, P11, P13, P14 and P19 shows a sharp decrease with increasing temperature and remains nearly constant after 200 K clearly shows an anomaly at ~ 200 K (see Fig. 4(a) and Fig.S5).

3.2.2 Discussion for phonon anomalies

The origin of the anomalies in phonon frequency, linewidth, and intensity near ~ 90 K, 140 K, and 200 K is not exactly pinpointed. The anomaly at ~ 90 K is suggestive of the development of short-range magnetic correlations. Previous magnetic susceptibility data show a broad maximum in the susceptibility well above T_N, which is typically associated with short-range ordering [19]. A related system, $AgCrP_2Se_6$, reports a substantial fraction of the entropy is released above the Néel temperature, suggesting that short-range ferromagnetic ordering exists above T_N, again hinting that short-range correlations could be possible in these types of systems [44]. Also, the exchange parameter for $AgCrP_2S_6$ is estimated to be of the order of J ~ 9meV (~ 100 K) [14]; therefore, the observed changes in the phonon modes around 90 K may be associated with the short-range ordering. We note that its sister compound, i.e. $CuCrP_2S_6$, undergoes antiferroelectric and antiferromagnetic ordering attributed to the Cu^+ and Cr^{3+}

View Article Online
DOI: 10.1039/D5TC03093E

cations, respectively. It undergoes a phase transition from a room temperature paraelectric state (space group $C2/c$ and point group C_{2h}) to a quasi-antipolar state at ~ 190 K (space group P_c and point group C_s). And with further lowering the temperature it goes to a fully antiferroelectric phase at ~ 145 K with space group P_c. This has been attributed to the ordering of Cu ions within the lamellae. Additionally, across the antipolar phase transition at ~ 145 K it shows negative thermal expansion [21]. On the other hand, for $AgCrP_2S_6$ it is advocated that since Ag^+ is a heavier cation, it will not dislocate in the lattice, and hence no ferroelectric transition is expected [45]. It is also possible that subtle local distortions associated with antipolar and quasi-antipolar order may exist, which could be reflected in localized probes such as Raman spectroscopy. Also, for $AgCrP_2Se_6$, two higher temperature transitions have been reported at ~ 68 K and 125 K, other than the low temperature antiferromagnetic transition at ~ 42 K [44]. The two transitions are attributed to the possible ferroelectric/antiferroelectric ordering due to lattice restructuring involving Ag ions. Also, a negative thermal expansion is reported around ~ 180 K. We note that Cu ion hopping is responsible for the ionic conductivity in $CuCrP_2S_6$. Ionic conductivity in $AgCrP_2S_6$ is low compared to the $CuCrP_2S_6$ as also reflected from their activation energy (1.26/0.67eV for (Ag/Cu)CrPS) [45]. The hopping of Ag ion in $AgCrP_2S_6$ cannot be ruled out, though the hopping may be limited and hence the possibility of an antipolar ordering similar to $CuCrP_2S_6$. Our observations of soft phonon like modes (discussed in detailed in Sec. 3.3) and observed anomalies in the phonon modes suggest that, despite the heaviness of Ag^+ ion, the antipolar and quasi-antipolar phase transitions cannot be ruled out in $AgCrP_2S_6$. Our observations suggest several contributing factors for this anomalous trend of the phonon modes, as discussed in Sec. 3.3. One possible explanation is that local structural contraction may be associated with the Ag^+ and Cr^{3+} cations structures. Nevertheless, our observations of distinct changes in modes frequency, linewidth, and intensity suggest the possibility of multiple phase transitions in the $AgCrP_2S_6$. So far, no transport measurements have been done on this material to confirm a ferroelectric transition. This is an important open question. Our observation calls for further theoretical and experimental studies to shed more light on the complex physics associated with this system, particularly the ambiguity surrounding the polar/anti-polar ordering and related phonon anharmonicities.

3.2.3 Emergence of new phonon modes at low temperature

Irreducible phonon mode calculations show that there are only 30 Raman active modes, but we have observed a total of 48 phonon modes at the lowest temperature, including some weak modes (see Table S1). As the temperature rises, several modes disappear, with the total number

View Article Online
DOI: 10.1039/D5TC03093E

reducing to nearly half, i.e. 27, of that observed at low temperature, as shown in Fig. S3. While decreasing the temperature we notice many new modes starts appearing in the temperature window of ~ 140-200 K, as expected for a first-order character of the antiferroelectric transition. We note that with increasing temperature from 6 K, modes involving dynamics of metal ions soften and broaden and finally disappear around 140-200 K. For example, low frequency mode P4 /P5, see Fig. 3/Fig. S4, soften by ~ 2.5/3% and disappear at ~ 140/200 K. The disappearance of these phonon modes along with many other modes with increasing temperature can be attributed to several factors, including thermal broadening, increased anharmonic phonon-phonon interactions, and reduced phonon lifetime, which results in an increase in FWHM. Additionally, structural instability in symmetry may also contribute to the suppression of certain modes at elevated temperatures [46]. As outlined in the review by S. Kamba [47], displacive ferroelectric transitions are typically characterized by the softening of optical phonon modes, where the frequency of the soft mode continuously decreases and ideally approaches zero at the critical temperature (T_C), indicating a lattice instability. In contrast, order-disorder transitions are governed by the relaxational dynamics of ions or dipoles hopping between equilibrium positions, and the characteristic frequency slowing is generally observed in the microwave to low-frequency regime rather than in the optical phonon spectrum. Here, we observed low-frequency soft phonon-like modes (P2, P3, P7, P10, P12, and P14) whose frequency decreases with decreasing temperature but does not approach zero at T_C, indicating the absence of a purely displacive mechanism. Observed phonon anomalies in phonon self-energy parameters, along with the emergence of new modes, suggest a more complex behaviour possibly involving structural transition and ordering of Ag ions within the lattice. This scenario points towards an order-disorder type transition with contributions from coupled lattice instabilities. A similar ambiguity exists in the case of $CuCrP_2S_6$, where an order-disorder transition is suggested [43], yet soft-mode-like features have been reported [48]. Therefore, it is likely that similar to its sister compound $CuCrP_2S_6$, $AgCrP_2S_6$ also undergoes order-disorder type of structural transition and is also responsible for the potential polar ordering.

Our observations clearly favour the possibility of structural instability, with singular changes in self-energy parameters of the prominent modes which survive at all the temperatures. We note that symmetry of the newly emerged modes at low temperature (see Fig. S12, S13) is also similar to the modes at high temperature. This reflects that symmetry of

View Article Online
DOI: 10.1039/D5TC03093E

the modes is same, but their number becomes nearly double i.e. going to the lower symmetry (C_2 or C_s) as temperature is decreased. Our observation of emergence of new modes in the temperature interval of ~ 140-200 K and modes showing distinct anomalies at these temperatures suggest a symmetry-lowering structural transition from a high temperature C_{2h} point group to C_2 or C_s point groups at these temperatures [21].

3.3 Discussion on anomalous hardening of the phonon modes

Anomalous hardening of the low frequency phonon modes P2, P3, P7, P10, P12 and P14 may be associated with the anharmonic effects which comes into the picture due to (i) Strong phonon-phonon anharmonic interactions and (ii) Lattice thermal contraction or structural instability, which are discussed as following:

(i) Strong phonon-phonon anharmonic interactions

Generally, with increasing temperature a phonon mode softens. However, a strong phonon-phonon anharmonic interactions may lead to phonon hardening with increasing temperature [49] and this abnormal phonon hardening in our case may also favour a possible transition based on the large atomic displacement i.e. antiferroelectric transition. These interactions play a crucial role in determining the ground state of incipient ferroelectrics. The self-energy of a phonon is given as: $\Sigma = \Sigma_r + i\Sigma_i$, imaginary part ($\Sigma_i$) is related to the lifetime of a phonon and for a given phonon, it is a function of ω and T given as: $\Delta\Gamma(T) \propto \Sigma_i(\omega) \propto |V|^2 \rho_2(\omega, T)$, where V is the average anharmonic coupling constant and $\rho_2(\omega)$ is the two-phonon density of states with the restrictions of momentum conservation and $\omega = \omega_1 + \omega_2$. The real part, Σ_r, is associated with the phonon frequency given as:

$$\Delta\omega(T) \propto \Sigma_r = \frac{2|V|^2}{\pi} \int_0^\infty \frac{\rho_2(\omega', T)}{\omega^2(T) - \omega'^2} \, \mathrm{d}\omega' , \qquad (1)$$

View Article Online
DOI: 10.1039/D5TC03093E

for simplicity, V is assumed as independent of frequency. The sign of this integral determines the sign of the self-energy constant (A), which is generally negative due to the dominance of the term with $\omega' > \omega$. Conversely, if the peak in the two-phonon density of states is lower than ω, the integral may give a positive value, potentially resulting in a hardening of the phonon modes [49,50]. Our observation of the anomalous hardening of the mode P2, P3, P7, P10, P12, and P14 clearly reflects strong phonon-phonon anharmonic interaction suggesting large movement of ions. We note that these low frequency modes are associated with the motion of heavy ions Ag^{+}/Cr^{3+}, and these ions are the ones where displacement is potentially responsible for the antiferroelectric transition in this class of material. Therefore, based on the anomalies observed here we also suggest that these anomalies in this system are potentially related with the potential antipolar ordering.

Now to understand the impact of anharmonicity on the frequency and FWHM of the phonon modes in the temperature range of ~ 140 to 300 K, we use anharmonic three-phonon model, given as [39,51]:

$$\Delta\omega = \omega(T) - \omega_0 = A\left(1 + \frac{2}{e^x - 1}\right), \qquad (2)$$

$$\Delta\Gamma = \Gamma(T) - \Gamma_0 = C\left(1 + \frac{2}{e^x - 1}\right), \qquad (3)$$

where ω_0 and Γ_0 represent the mode frequency and FWHM at absolute zero temperature, respectively, and $x = \frac{\hbar\omega_0}{2k_BT}$. A and C represent the self-energy constant that describe the strength of phonon-phonon interactions involving three phonon processes. Anharmonic model fit to the experimental data for the case of frequency and FWHM is shown by solid red lines in the temperature range of 140-300 K. Figure 3 illustrates prominent modes fitted (frequency and FWHM) using equations (2) and (3), respectively. The optimal parameters are shown in Table S3. The self-energy constant (A) associated with mode P2 and

View Article Online
DOI: 10.1039/D5TC03093E

P10 is positive, indicating that term $\omega > \omega'$ is dominant in equation (1) for these modes, while for all other phonon modes it is negative.

(ii) Lattice thermal contraction or structural instability

Temperature-dependent behaviour of the phonon modes is closely related to the direction (symmetry) and magnitude of lattice vibrations; anomalous phonon mode behaviour may arise from their anisotropic structural properties. Hardening of the low frequency phonon modes with increasing temperature indicates that bonding stiffness corresponding to these modes increases, suggesting that there may be a local structural instability [52]. This type of behaviour of phonon modes is referred to as soft phonon modes, i.e., their frequency decreases with decreasing temperature. The soft mode like behaviour is understood within the mean field approximation [43,53] $\omega(T) = \beta(T^* - T)^{1/2} + \omega_0$, where β is constant and T^* is the characteristic temperature at which a mode disappears. As clear from our observation T^* is found to be in the range of ~ 140-200 K. We note that frequency of these modes does not go to zero across T^*, unlike the soft phonon mode expected in a displacive-type structural transition. The presence of second term ω_0 favours the view point that quasi-antipolar order is also present in this system similar to compound $CuCrP_2S_6$ and is driven by an order-disorder transition rather than the condensation of a soft phonon mode. Many of the low frequency phonon modes (P2, P3, P7, P10, P12, and P14; see Fig. 3) associated with motion of metal cations shows anomalous softening. This anomalous behaviour may be associated with the interlayer silver ion hopping. We note that similar behaviour is also reported for a phonon mode in $CuCrP_2S_6$ [43]. Therefore, our observations of anomalous softening of the low frequency modes in $AgCrP_2S_6$ suggest the possibility of quasi-antiferroelectric and subsequently antiferroelectric ordering in the temperature window of ~ 200-140 K.

3.4 Fano resonance

View Article Online
DOI: 10.1039/D5TC03093E

We observed that the phonon mode P31 exhibits an asymmetric line shape, which can be attributed to the interaction between the discrete phonon and an underlying magnetic or electronic continuum. In $AgCrP_2S_6$, an electronic origin of the continuum can be ruled out, since the optical band gap lies far above the Raman excitation energy (~1.32 eV at 6 K), making the electronic contribution negligible. Therefore, the continuum responsible for the Fano asymmetry is most likely magnetic in nature. This suggests that the asymmetric profile of the P31 mode originates from magnetic fluctuations within the Cr sublattice, indicative of a spin-phonon coupling mechanism. Such asymmetry is well described by the Breit-Wigner-Fano (BWF) function as [54]: $I(\omega) = I_0 \frac{[1+(\omega-\omega_0)/q\Gamma]^2}{1+[(\omega-\omega_0)/\Gamma]^2}$, where ω_0 and Γ are the frequency and FWHM of uncoupled phonon, respectively. q is the asymmetry parameter that characterizes the coupling strength between the phonon and the continuum, quantified by the parameter $1/|q|$. Microscopically $1/|q| \propto |V_E|$, where $|V_E|$ tells the interaction between the discrete state and the continuum. Therefore, limit $1/|q| \to 0$ corresponds to weak coupling, which causes the peak to be symmetric and reduces to a Lorentzian line shape; and limit $1/|q| \to \infty$ represents strong coupling that causes the peak to be more asymmetric. Figure 4(c-i) shows the temperature evolution of asymmetric mode P31 in the temperature range of 6-300 K. Figures 4(c-ii) and (c-iii) show the temperature dependence of the frequency and FWHM of mode P31 in the temperature range of 6-200 K. For mode P31, as the temperature increases, the frequency decreases and the FWHM increases, with a change in slope for both parameters occurring around T_N (~ 20 K). Figure 4(c-iv) shows the temperature dependence of the coupling strength (1/|q|), and it decreases with increase in temperature with a jump around T_N (~ 20 K). This

View Article Online
DOI: 10.1039/D5TC03093E

suggests the coupling between phonon and underlying magnetic continuum is strongly affected by long-range magnetic ordering.

4. Polarization dependence of the phonon modes

To determine the symmetry and to understand the angle-dependent characteristics of the phonon modes, we carried out an in-depth polarization-dependent Raman measurements at four temperatures: 6 K, 60 K, 120 K, and 170 K as shown in Fig. 5 for few selected modes (for more phonon modes see Supplemental Material Fig. S10 and Fig. S11 [15]). The angular dependence of the phonon modes intensity is given by eqn (4) and (5), considering the complex element of the Raman tensor (see Sec. S1 in Supplemental Material for polarization intensity analysis details [15])

$$I_{A_g} = |b|^2 \cos^2(\theta+\theta_0)\cos^2\theta_0 + |c|^2 \sin^2(\theta+\theta_0)\sin^2\theta_0 + 2|b||c|\cos(\theta+\theta_0)\cos\theta_0 \sin(\theta+\theta_0)\sin\theta_0 \cos\phi_{bc} \quad (4)$$

$$I_{B_g} = |f|^2 \sin^2(\theta+2\theta_0), \quad (5)$$

where $\phi_{bc} = \phi_b - \phi_c$ is the phase difference between b and c components of the Raman tensor.

In Fig. 5 (Supplemental Material Fig. S10 and Fig. S11 [15]) solid red line shows the fitted curves using eqn (4) and (5).

Figure 5 shows the polar plot for the intensity of the modes P7, P8, P13, P19, and P47 at four different temperatures. Mode P7 shows the quasi-isotropic behaviour at 6 K, and it approaches two-fold symmetry at 60 K; and it shows complete two-fold symmetry at higher temperatures 120 and 170 K with maxima around 20 and 200 degrees. Mode P8 shows the two-fold symmetry at all four temperatures, with maxima around 40 and 220 degrees. Mode P47 shows the quasi-isotropic behaviour at 6 and 60 K, while it becomes two-fold at 120 and 170 K with maxima around 20 and 200 degrees. The modes that disappeared at higher temperatures

View Article Online
DOI: 10.1039/D5TC03093E

also exhibit twofold symmetry, as shown in Supplemental Material Fig. S12 and Fig. S13 [51]. This reflects that symmetry of these modes is also A_g/B_g or A/B consistent with the group theoretical arguments. Interestingly, mode P13 shows the quasi-isotropic behaviour with maxima around 40 and 220 degrees at 6 and 60 K, while at higher temperatures 120 and 170 K, it shows the maxima around 90 and 270 degrees. Also, mode P19 and P33 (see Fig. S11) shows maxima at ~ 140 and 320 degrees at 6 and 60 K, while at higher temperatures it shows maxima ~ 0 and 180 degrees. Such rotation in the polar plots likely originates from subtle structural changes or distortions that modify the Raman tensor elements at lower temperatures. The magneto-optical Kerr effect can be ruled out as the primary cause, since the observed rotation is not uniform across all phonon modes and occurs well above the magnetic ordering temperature, where long-range magnetic order is absent. The possibility of birefringence-induced rotation is also less probable, as the effect is strongly mode-selective and does not show the uniform angular dependence characteristic of optical birefringence. Instead, a more probable origin could be strain-induced local anisotropy or temperature-driven structural distortion, both of which can locally modify the polarizability tensor and give rise to the observed rotation in certain phonon modes. We note that similar rotation has also been reported recently in other 2D magnetic systems [5,55]. The microscopic understanding of these rotations and change in the symmetry from quasi-isotropic behaviour to twofold symmetry as a function of temperature calls for a detailed theoretical study to uncover underlying mechanisms responsible for these changes.

5. Conclusion

In conclusion, we performed a comprehensive temperature- and polarization-dependent Raman measurements on single crystal $AgCrP_2S_6$ along with the first-principle based calculations of the phonons. Our results have shown that this quasi 2D van der Waals material, $AgCrP_2S_6$, with 1D spin chains demonstrate a possibility of quasi-antipolar and antipolar phase transition

View Article Online
DOI: 10.1039/D5TC03093E

opposite to the conventional view so far adopted in the literature, therefore putting forward that even the heavy ion (Ag) based system may show antiferroelectric ordering. Our findings also pave the way forward for potential controlling and manipulating these ordering as a function of layer and make them useful for potential applications. We also observed signature of a long-range magnetic ordering at low temperature, all these transitions are marked by the distinct renormalization of the phonon modes as well as emergence of multiple phonon modes with decreasing temperature. Our findings also point that this material may also be tuned as a potential multiferroic material similar to its sister compounds. Additionally, polarization-dependent measurements elucidate the role of anisotropy in the system, shedding light on the crystal symmetry. Our findings offer critical insights into the phonon dynamics of this quasi-2D magnetic compound, providing a deeper understanding of its underlying mechanisms.

Author contributions

Chaitanya B. Auti: writing, review and editing, writing - original draft, investigation, data curation, formal analysis, methodology. Atul G. Chakkar: data curation, formal analysis, writing - review & editing. Shantanu Semwal: data curation, formal analysis, writing - review & editing. Sebastian Selter: formal analysis, writing - review & editing. Yuliia Shemerliuk: formal analysis, writing - review & editing. Bernd Büchner: formal analysis, writing - review & editing. Saicharan Aswartham: formal analysis, writing - review & editing. Koushik Pal: data curation, formal analysis, writing - review & editing. Pradeep Kumar: formal analysis, funding acquisition, supervision, validation, methodology, writing - review & editing.

Conflicts of interest

There are no conflicts to declare.

Data availability statement

View Article Online
DOI: 10.1039/D5TC03093E

All data that supports the findings of this study are included within the article and supplementary file.

Acknowledgements

P.K. thanks SERB (Project no. CRG/2023/002069) for the financial support and IIT Mandi for the experimental facilities.

References:

[1] C. Liu, H. Chen, S. Wang, Q. Liu, Y.-G. Jiang, D. W. Zhang, M. Liu, and P. Zhou, Two-dimensional materials for next-generation computing technologies, Nat. Nanotechnol. **15**, 545 (2020).

[2] L. Liao, E. Kovalska, J. Regner, Q. Song, and Z. Sofer, Two-Dimensional Van Der Waals Thin Film and Device, Small **20**, 2303638 (2024).

[3] T. T. Mai, K. F. Garrity, A. McCreary, J. Argo, J. R. Simpson, V. Doan-Nguyen, R. V. Aguilar, and A. R. H. Walker, Magnon-phonon hybridization in 2D antiferromagnet $MnPSe_3$, Sci. Adv. **7**, eabj3106 (2021).

[4] S. Liu, A. Granados del Águila, D. Bhowmick, C. K. Gan, T. Thu Ha Do, M. A. Prosnikov, D. Sedmidubský, Z. Sofer, P. C. M. Christianen, and P. Sengupta, Direct observation of magnon-phonon strong coupling in two-dimensional antiferromagnet at high magnetic fields, Phys. Rev. Lett. **127**, 097401 (2021).

[5] A. G. Chakkar, D. Kumar, and P. Kumar, Broken weak and strong spin rotational symmetries and tunable interactions between phonons and the continuum in $Cr_2Ge_2Te_6$, Phys. Rev. B **109**, 134406 (2024).

[6] N. Khan, D. Kumar, V. Kumar, Y. Shemerliuk, S. Selter, B. Büchner, K. Pal, S. Aswartham, and P. Kumar, The interplay of topology and antiferromagnetic order in two-dimensional van der Waals crystals of $(Ni_xFe_{1-x})_2P_2S_6$, 2D Mater. **11**, 035018 (2024).

[7] H. Li, S. Ruan, and Y.-J. Zeng, Intrinsic Van Der Waals Magnetic Materials from Bulk to the 2D Limit: New Frontiers of Spintronics, Adv. Mater. **31**, 1900065 (2019).

[8] S. Kumari, D. K. Pradhan, N. R. Pradhan, and P. D. Rack, Recent developments on 2D magnetic materials: challenges and opportunities, Emerg. Mater. **4**, 827 (2021).

[9] P. Joy and S. Vasudevan, Magnetism in the layered transition-metal thiophosphates MPS_3 (M= Mn, Fe, and Ni), Phys. Rev. B **46**, 5425 (1992).

[10] A. R. Wildes, S. J. Kennedy, and T. J. Hicks, True two-dimensional magnetic ordering in $MnPS_3$, J. Phys.: Condens. Matter **6**, L335 (1994).

[11] R. Samal, G. Sanyal, B. Chakraborty, and C. S. Rout, Two-dimensional transition metal phosphorous trichalcogenides (MPX_3): a review on emerging trends, current state and future perspectives, J. Mater. Chem. A **9**, 2560 (2021).

[12] P. Colombet, A. Leblanc, M. Danot, and J. Rouxel, Structural aspects and magnetic properties of the lamellar compound $Cu_{0.50}Cr_{0.50}PS_3$, J. Solid State Chem. **41**, 174 (1982).

[13] S. Lee, P. Colombet, G. Ouvrard, and R. Brec, A new chain compound of vanadium (III): $Ag_{12}V_{12}PS_3$ structure, metal ordering, and magnetic properties, Mater. Res. Bull. **21**, 917 (1986).

[14] H. Mutka, C. Payen, and P. Molinié, One-Dimensional Heisenberg Antiferromagnet with Spin S = 3/2. Experiments on $AgCrP_2S_6$, Europhys. Lett. **21**, 623 (1993).

[15] See Supplemental Material at [URL will be inserted by publisher] for analysis of polarization dependent intensity; temperature-dependent photoluminescence; crystal structure; fitted Raman spectrum; temperature dependent frequency, FWHM, intensity of phonon modes; magnified temperature dependent Raman spectrum; polarization dependence of phonon modes; schematic for polarization configuration; mode visualization, and related tables. The Supplemental Material also contains Refs. [56-67].

[16] M. A. Susner, M. Chyasnavichyus, M. A. McGuire, P. Ganesh, and P. Maksymovych, Metal Thio- and Selenophosphates as Multifunctional van der Waals Layered Materials, Adv. Mater. **29**, 1602852 (2017).

[17] R. Brec, Review on structural and chemical properties of transition metal phosphorous trisulfides MPS_3, Solid State Ionics **22**, 3 (1986).

[18] C. Payen, P. Molinie, P. Colombet, and G. Fillion, Powder and single crystal susceptibility of the quasi-1D Heisenberg antiferromagnetic chain compounds $AgVP_2S_6$ (S = 1) and $AgCrP_2S_6$ (S = 3/2), J. Magn. Magn. Mater. **84**, 95 (1990).

[19] E. Park, J. P. Philbin, H. Chi, J. J. Sanchez, C. Occhialini, G. Varnavides, J. B. Curtis, Z. Song, J. Klein, J. D. Thomsen, M.-G. Han, A. C. Foucher, K. Mosina, D. Kumawat, N. Gonzalez-Yepez, Y. Zhu, Z. Sofer, R. Comin, J. S. Moodera, P. Narang, and F. M. Ross, Anisotropic 2D van der Waals Magnets Hosting 1D Spin Chains, Adv. Mater. **36**, 2401534 (2024).

[20] K. Kim, S. Y. Lim, J.-U. Lee, S. Lee, T. Y. Kim, K. Park, G. S. Jeon, C.-H. Park, J.-G. Park, and H. Cheong, Suppression of magnetic ordering in XXZ-type antiferromagnetic monolayer $NiPS_3$, Nat. Commun. **10**, 345 (2019).

[21] M. A. Susner, R. Rao, A. T. Pelton, M. V. McLeod, and B. Maruyama, Temperature-dependent Raman scattering and x-ray diffraction study of phase transitions in layered multiferroic $CuCrP_2S_6$, Phys. Rev. Mater. **4**, 104003 (2020).

[22] R. Rao, R. Selhorst, B. S. Conner, and M. A. Susner, Ferrielectric-paraelectric phase transitions in layered $CuInP_2S_6$ and $CuInP_2S_6$-$In_{4/3}P_2S_6$ heterostructures: A Raman spectroscopy and x-ray diffraction study, Phys. Rev. Mater. **6**, 045001 (2022).

[23] V. Kumar, D. Kumar, B. Singh, Y. Shemerliuk, M. Behnami, B. Büchner, S. Aswartham, and P. Kumar, Fluctuating fractionalized spins in quasi-two-dimensional magnetic $V_{0.85}PS_3$, Phys. Rev. B **107**, 094417 (2023).

[24] B. Singh, D. Kumar, V. Kumar, M. Vogl, S. Wurmehl, S. Aswartham, B. Büchner, and P. Kumar, Fractional spin fluctuations and quantum liquid signature in Gd_2ZnIrO_6, Phys. Rev. B **104**, 134402 (2021).

[25] X. Wang, Z. Shang, C. Zhang, J. Kang, T. Liu, X. Wang, S. Chen, H. Liu, W. Tang, Y.-J. Zeng, J. Guo, Z. Cheng, L. Liu, D. Pan, S. Tong, B. Wu, Y. Xie, G. Wang, J. Deng, T. Zhai, H.-X. Deng, J. Hong, and J. Zhao, Electrical and magnetic anisotropies in van der Waals multiferroic $CuCrP_2S_6$, Nat. Commun. **14**, 840 (2023).

[26] P. T. Orban, S. M. Bernier, T. Berry, M. A. Siegler, and T. M. McQueen, Random-exchange Heisenberg behavior in the electron-doped quasi-one-dimensional spin-1 chain compound $AgVP_2S_6$, Phys. Rev. B **110**, 054423 (2024).

[27] X. Wang, C. Zhu, Y. Deng, R. Duan, J. Chen, Q. Zeng, J. Zhou, Q. Fu, L. You, S. Liu, J. H. Edgar, P. Yu, and Z. Liu, Van der Waals engineering of ferroelectric heterostructures for long-retention memory, Nat. Commun. **12**, 1109 (2021).

[28] Y. Ma, Y. Yan, L. Luo, S. Pazos, C. Zhang, X. Lv, M. Chen, C. Liu, Y. Wang, A. Chen, Y. Li, D. Zheng, R. Lin, H. Algaidi, M. Sun, J. Z. Liu, S. Tu, H. N. Alshareef, C. Gong, M. Lanza, F. Xue, and X. Zhang, High-performance van der Waals antiferroelectric $CuCrP_2S_6$-based memristors, Nat. Commun. **14**, 7891 (2023).

[29] S. Selter, Y. Shemerliuk, B. Büchner, and S. Aswartham, Crystal Growth of the Quasi-2D Quarternary Compound $AgCrP_2S_6$ by Chemical Vapor Transport, Crystals **11** (2021).

[30] G. Kresse and J. Furthmüller, Efficient iterative schemes for ab initio total-energy calculations using a plane-wave basis set, Phys. Rev. B **54**, 11169 (1996).

[31] G. Kresse and D. Joubert, From ultrasoft pseudopotentials to the projector augmented-wave method, Phys. Rev. B **59**, 1758 (1999).

[32] P. E. Blöchl, Projector augmented-wave method, Phys. Rev. B **50**, 17953 (1994).

View Article Online
DOI: 10.1039/D5TC03093E

[33] J. P. Perdew, K. Burke, and M. Ernzerhof, Generalized gradient approximation made simple, Phys. Rev. lett. **77**, 3865 (1996).

[34] S. Grimme, J. Antony, S. Ehrlich, and H. Krieg, A consistent and accurate ab initio parametrization of density functional dispersion correction (DFT-D) for the 94 elements H-Pu, J. Chem. Phys. **132**, 154104 (2010).

[35] A. Togo, L. Chaput, T. Tadano, and I. Tanaka, Implementation strategies in phonopy and phono3py, J. Phys.: Condens. Matter **35**, 353001 (2023).

[36] A. Togo, First-principles phonon calculations with phonopy and phono3py, J. Phys. Soc. Jpn. **92**, 012001 (2023).

[37] D. L. Rousseau, R. P. Bauman, and S. P. S. Porto, Normal mode determination in crystals J. Raman Spectrosc. **10**, 253 (1981).

[38] M. Bernasconi, G. Marra, G. Benedek, L. Miglio, M. Jouanne, C. Julien, M. Scagliotti, and M. Balkanski, Lattice dynamics of layered MPX_3 (M= Mn, Fe, Ni, Zn; X= S, Se) compounds, Phys. Rev. B **38**, 12089 (1988).

[39] M. Balkanski, R. F. Wallis, and E. Haro, Anharmonic effects in light scattering due to optical phonons in silicon, Phys. Rev. B **28**, 1928 (1983).

[40] D. J. Lockwood and M. G. Cottam, The spin-phonon interaction in FeF_2 and MnF_2 studied by Raman spectroscopy, J. Appl. Phys. **64**, 5876 (1988).

[41] A. Ghosh, M. Palit, S. Maity, V. Dwij, S. Rana, and S. Datta, Spin-phonon coupling and magnon scattering in few-layer antiferromagnetic $FePS_3$, Phys. Rev. B **103**, 064431 (2021).

[42] B. Zhang, Y. Hou, Z. Wang, and R. Wu, First-principles studies of spin-phonon coupling in monolayer $Cr_2Ge_2Te_6$, Phys. Rev. B **100**, 224427 (2019).

[43] K. Cho, S. Lee, R. Kalaivanan, R. Sankar, K. Y. Choi, and S. Park, Tunable ferroelectricity in van der Waals layered antiferroelectric $CuCrP_2S_6$, Adv. Funct. Mater. **32**, 2204214 (2022).

[44] M. A. Susner, B. S. Conner, E. Rowe, R. Siebenaller, A. Giordano, M. V. McLeod, C. R. Ebbing, T. J. Bullard, R. Selhorst, and T. J. Haugan, Structural, Magnetic, and Optical Properties of the van der Waals Antiferromagnet $AgCrP_2Se_6$, J. Phys. Chem. C **128**, 4265 (2024).

[45] I. Zamaraite, A. Dziaugys, J. Banys, and Y. Vysochanskii, Dielectric and electrical properties of $AgCrP_2S_6$ and $Cu_{0.2}Ag_{0.8}CrP_2S_6$ layered crystals, Ferroelectrics **515**, 13 (2017).

[46] D. Fausti, A. A. Nugroho, P. H. van Loosdrecht, S. A. Klimin, M. N. Popova, and L. N. Bezmaternykh, Raman scattering from phonons and magnons in $RFe_3(BO_3)_4$, Phys. Rev. B **74**, 024403 (2006).

[47] S. Kamba, Soft-mode spectroscopy of ferroelectrics and multiferroics: A review, APL Mater. **9**, 020704 (2021).

[48] J. Tang, B. J. Lawrie, M. Cheng, Y.-C. Wu, H. Zhao, D. Kong, R. Lu, C.-H. Yao, Z. Gai, and A.-P. Li, Raman Fingerprints of Phase Transitions and Ferroic Couplings in van der Waals Multiferroic $CuCrP_2S_6$, J. Phys. Chem. Lett. **16**, 4336 (2025).

[49] M. Cardona and T. Ruf, Phonon self-energies in semiconductors: anharmonic and isotopic contributions, Solid State Commun. **117**, 201 (2001).

[50] B. Singh, G. A. Cansever, T. Dey, A. Maljuk, S. Wurmehl, B. Büchner, and P. Kumar, Orbiton–phonon coupling in $Ir^{5+}(5d^4)$ double perovskite Ba_2YIrO_6, J. Phys.: Condens. Matter **31**, 065603 (2019).

[51] P. G. Klemens, Anharmonic Decay of Optical Phonons, Phys. Rev. B **148**, 845 (1966).

[52] Y. S. Lee, T. W. Noh, J. H. Park, K. B. Lee, G. Cao, J. E. Crow, M. K. Lee, C. B. Eom, E. J. Oh, and I.-S. Yang, Temperature-dependent Raman spectroscopy in $BaRuO_3$ systems, Phys. Rev. B **65**, 235113 (2002).

[53] J. Scott, Soft-mode spectroscopy: Experimental studies of structural phase transitions, Rev. Mod. Phys. **46**, 83 (1974).

[54] U. Fano, Effects of configuration interaction on intensities and phase shifts, Phys. Rev. **124**, 1866 (1961).

[55] B. Huang, J. Cenker, X. Zhang, E. L. Ray, T. Song, T. Taniguchi, K. Watanabe, M. A. McGuire, D. Xiao, and X. Xu, Tuning inelastic light scattering via symmetry control in the two-dimensional magnet CrI_3, Nat. Nanotechnol. **15**, 212 (2020).

[56] R. Loudon, The Raman effect in crystals, Adv. Phys. **13**, 423 (1964).

[57] J. Kim, J.-U. Lee, and H. Cheong, Polarized Raman spectroscopy for studying two-dimensional materials, J. Phys.: Condens. Matter **32**, 343001 (2020).

[58] V. Funk, K. Wagner, E. Wietek, J. D. Ziegler, J. Förste, J. Lindlau, M. Förg, K. Watanabe, T. Taniguchi, and A. Chernikov, Spectral asymmetry of phonon sideband luminescence in monolayer and bilayer WSe_2, Phys. Rev. Research **3**, L042019 (2021).

[59] A. Boziki, M. I. Dar, G. Jacopin, M. Gratzel, and U. Rothlisberger, Molecular origin of the asymmetric photoluminescence spectra of $CsPbBr_3$ at low temperature, J. Phys. Chem. Lett. **12**, 2699 (2021).

[60] J. Diouri, J. P. Lascaray, and M. E. Amrani, Effect of the magnetic order on the optical-absorption edge in $Cd_{1-x}Mn_xTe$, Phys. Rev. B **31**, 7995 (1985).

[61] Y. P. Varshni, Temperature dependence of the energy gap in semiconductors, Physica **34**, 149 (1967).

[62] R. Pässler, Basic model relations for temperature dependencies of fundamental energy gaps in semiconductors Phys. Status Solidi B **200**, 155 (1997).

[63] P. Lautenschlager, M. Garriga, S. Logothetidis, and M. Cardona, Interband critical points of GaAs and their temperature dependence, Phys. Rev. B **35**, 9174 (1987).

[64] C. Yu, Z. Chen, J. J Wang, W. Pfenninger, N. Vockic, J. T. Kenney, and K. Shum, Temperature dependence of the band gap of perovskite semiconductor compound $CsSnI_3$, J. Appl. Phys. **110**, 063526 (2011).

[65] S. Wang, J. Ma, W. Li, J. Wang, H. Wang, H. Shen, J. Li, J. Wang, H. Luo, and D. Li, Temperature-dependent band gap in two-dimensional perovskites: Thermal expansion interaction and electron–phonon interaction, J. Phys. Chem. Lett. **10**, 2546 (2019).

[66] S. Rudin, T. Reinecke, and B. Segall, Temperature-dependent exciton linewidths in semiconductors, Phys. Rev. B **42**, 11218 (1990).

[67] M. Leroux, N. Grandjean, B. Beaumont, G. Nataf, F. Semond, J. Massies, and P. Gibart, Temperature quenching of photoluminescence intensities in undoped and doped GaN, J. Appl. Phys. **86**, 3721 (1999).

View Article Online
DOI: 10.1039/D5TC03093E

Figures:

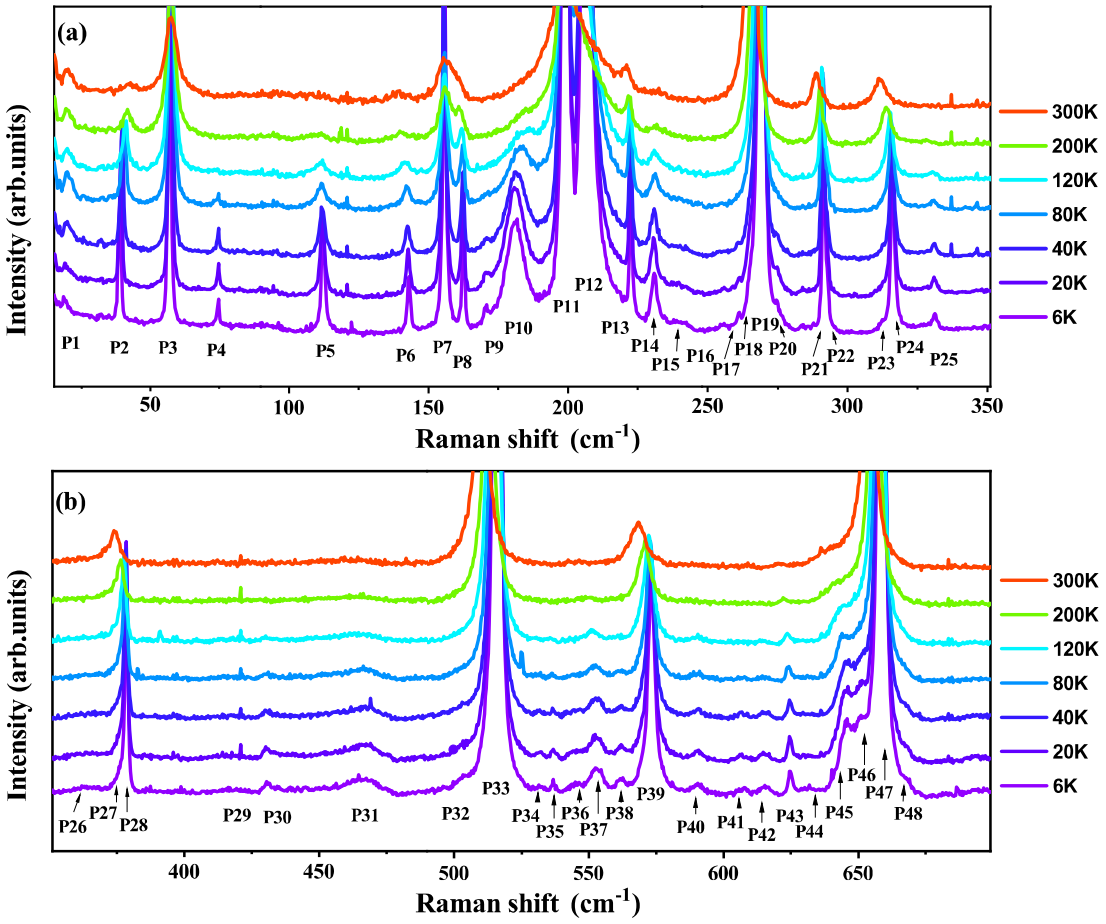

Figure 1. Temperature evolution of the Raman spectrum in the temperature range of 6 to 300 K, ranging from **(a)** 15-350 cm^{-1} and **(b)** 350-700 cm^{-1}. The observed phonon modes are labelled as P1-P48.

View Article Online
DOI: 10.1039/D5TC03093E

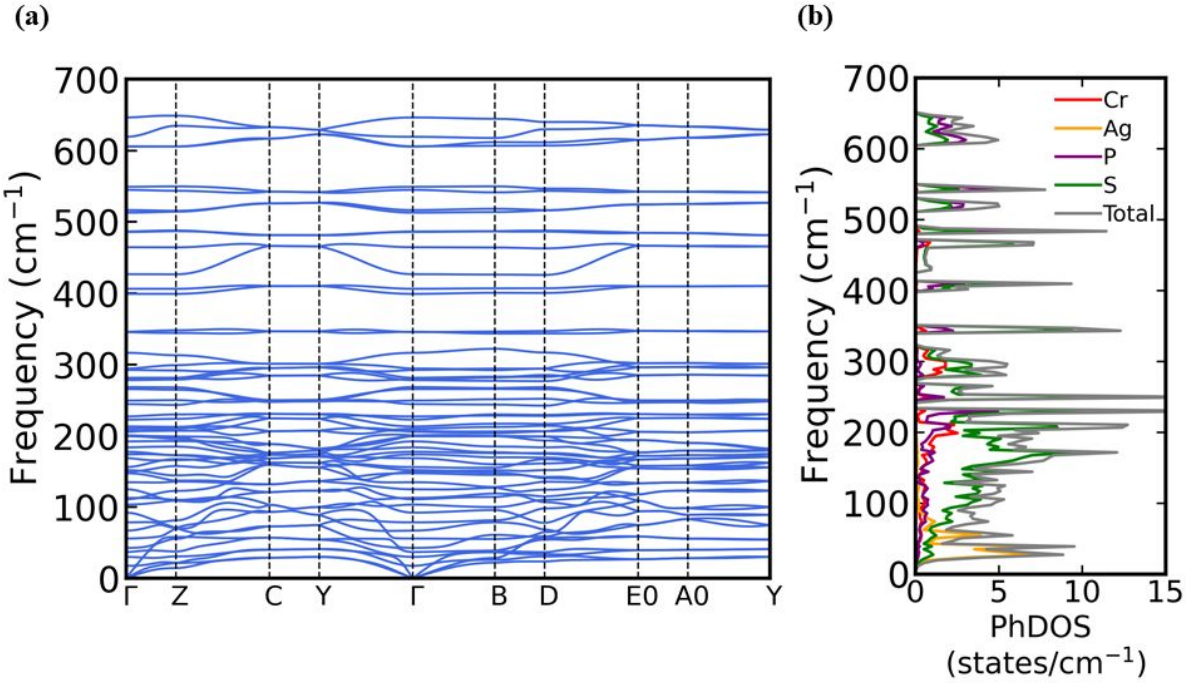

Figure 2. (a) Phonon dispersion and **(b)** atom resolved phonon density of states considering the AFM arrangement of $AgCrP_2S_6$ and including the vdW forces.

View Article Online
DOI: 10.1039/D5TC03093E

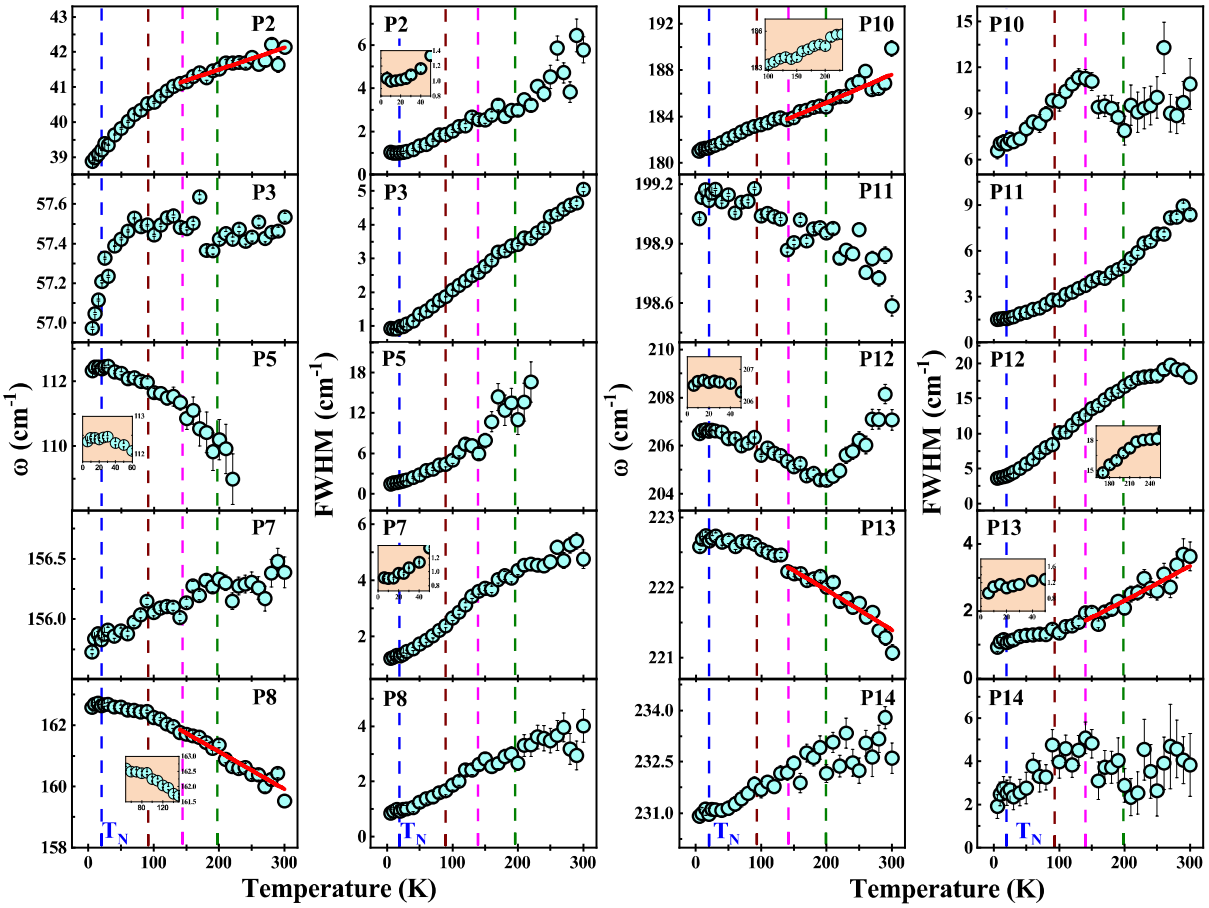

Figure 3. Temperature evolution of the mode frequency and FWHM of phonon modes P2, P3, P5, P7, P8, and P10-P14. The solid red line shows a three-phonon fitting in the temperature range 140 K to 300 K. The dashed blue line indicates the antiferromagnetic transition at T_N ~ 20 K. The dashed blue line marks the antiferromagnetic transition near ~ 20 K, while the dashed brown, pink, and green lines indicate anomalies around ~ 90 K, ~ 140 K, and ~ 200 K, respectively. The insets show magnified views of the corresponding anomalies in both frequency and FWHM.

View Article Online
DOI: 10.1039/D5TC03093E

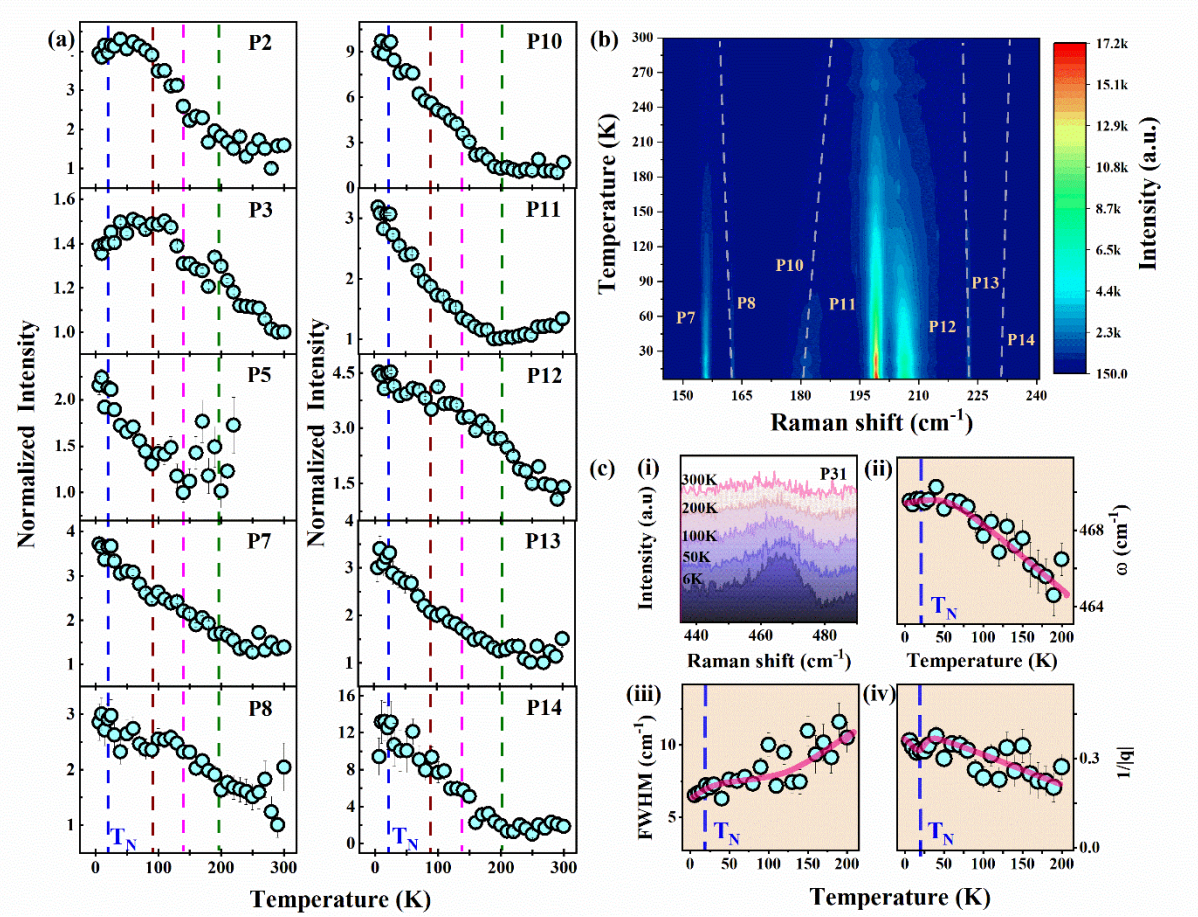

Figure 4. (a) Shows temperature dependence of the normalised intensity of modes P2, P3, P5, P7, P8, and P10-P14. **(b)** Shows a colour contour plot of the phonon intensity in the temperature-Raman-shift plane. The vertical dashed line marks the corresponding mode evolution. **(c)**-(i) Shows the temperature evolution of the Fano mode P31. (ii-iv) Shows the temperature dependence of the frequency, FWHM and the coupling strength (1/|q|) in the temperature range of 6 K to 200 K. The solid semi-transparent pink line is drawn as guide to the eye.

View Article Online
DOI: 10.1039/D5TC03093E

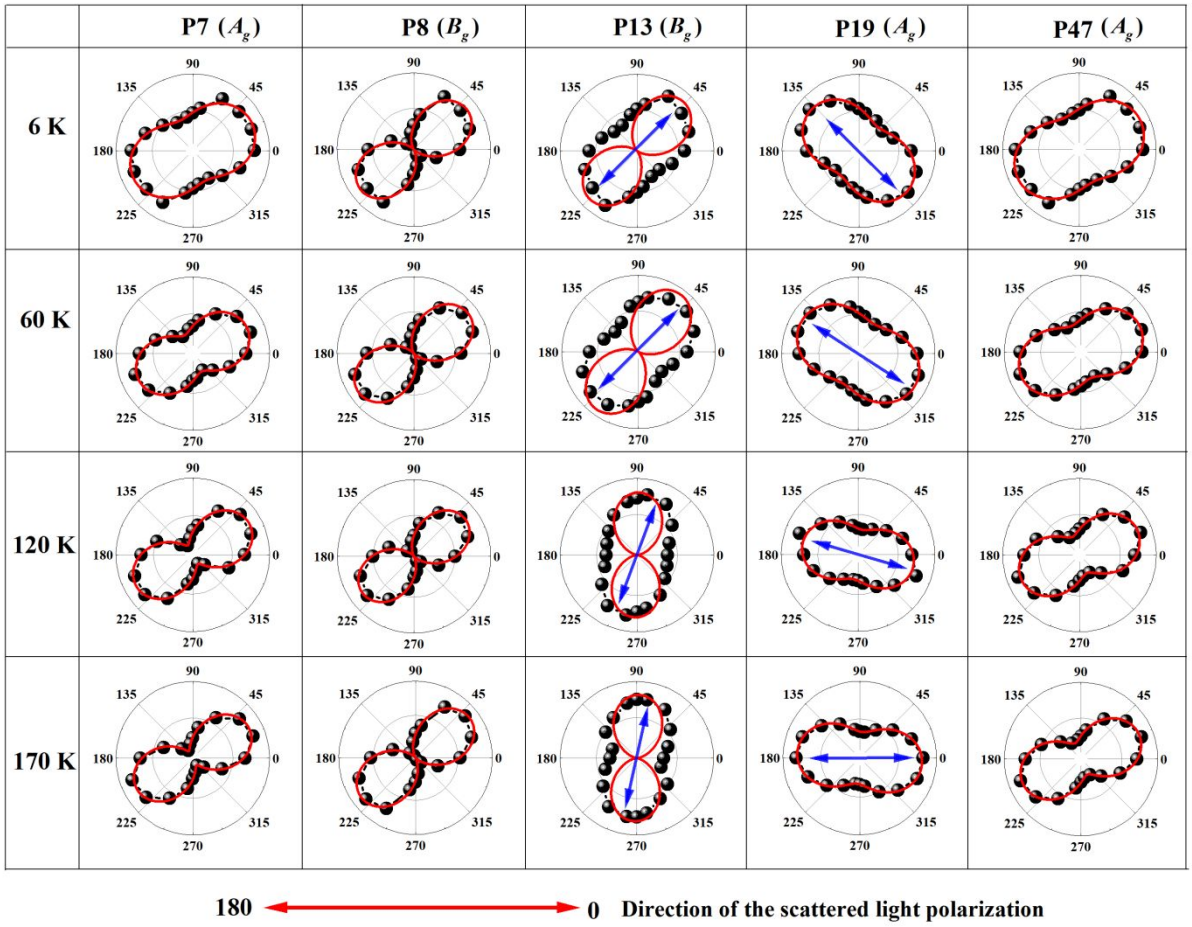

Figure 5. Polarization-dependent intensity profiles of phonon modes P7, P8, P13, P19, and P47 measured at 6 K, 60 K, 120 K, and 170 K, respectively, under varying incident-light polarization. Blue arrows represent the rotation of the axis, showing the maxima as a function of temperature. The solid red line at the bottom indicates the direction of the scattered light polarization.

View Article Online
DOI: 10.1039/D5TC03093E

Tables:

Table I.

Wyckoff positions of atoms and irreducible representations of the phonon modes for $AgCrP_2S_6$ in the monoclinic (P2/a; #13) crystal system.

Atoms	Wyckoff position	Mode decomposition	Raman tensors
Ag	2*e*	$A_g + A_u + 2B_g + 2B_u$	$A_g = \begin{pmatrix} b & 0 & d \\ 0 & c & 0 \\ d & 0 & a \end{pmatrix}$ $B_g = \begin{pmatrix} 0 & f & 0 \\ f & 0 & e \\ 0 & e & 0 \end{pmatrix}$
Cr	2*e*	$A_g + A_u + 2B_g + 2B_u$	
P	4 *g*	$3A_g + 3A_u + 3B_g + 3B_u$	
S	4 *g*	$3A_g + 3A_u + 3B_g + 3B_u$	
S	4 *g*	$3A_g + 3A_u + 3B_g + 3B_u$	
S	4 *g*	$3A_g + 3A_u + 3B_g + 3B_u$	
$\Gamma_{total} = 14A_g + 14A_u + 16B_g + 16B_u;$ $\Gamma_{Raman} = 14A_g + 16B_g;\ \Gamma_{IR} = 13A_u + 14B_u;\ \Gamma_{Acoustic} = A_u + 2B_u$			

Data availability statement

View Article Online
DOI: 10.1039/D5TC03093E

All data that supports the findings of this study are included within the article and supplementary file.